Eur. Phys. J. B **59**, 179–184 (2007)
DOI: 10.1140/epjb/e2007-00286-0

THE EUROPEAN PHYSICAL JOURNAL B

Trifurcation of band-gap structure and coexistence of lattice-like states and critical states in piezoelectric period-doubling superlattices

Z.X. Liu[a], L.M. Wang, H. He, and W.Y. Zhang

National Laboratory of Solid State Microstructures and Department of Physics, Nanjing University, 210093 Nanjing, P.R. China

Received 9 April 2007 / Received in final form 6 August 2007
Published online 17 October 2007 –

Abstract. We study the propagation of electromagnetic wave in piezoelectric period-doubling superlattices with using the generalized 4×4 transfer matrix method, and the dynamics of electromagnetic wave and acoustic wave is treated on equal footing. The band-gap structure trifurcates, which is understood within the framework of perturbation theory under periodic boundary condition. The uncoupled phononic branch of field distributions is Bloch-wave-like. For the coupled polaritonic branch, the lattice-like field distributions, for which Thue-Morse sequence is famous, also manifest in this piezoelectric period-doubling system and coexist with critical states. They can be characterized as extended if the superlattice size considered is large enough. In fact, our study suggests that such lattice-like field distributions are common phenomena in piezoelectric superlattices irrespective of lattice types and depend only on the frequency and domain widths, they reflect the intrinsic symmetry of the transfer matrices for the particular domain setting and frequency.

PACS. 41.20.Jb Electromagnetic wave propagation; radiowave propagation – 62.30.+d Mechanical and elastic waves; vibrations – 78.66.-w Optical properties of specific thin films

Ever since the experimental discovery of quasicrystal phase in an Al-Mn alloy with icosahedral symmetry [1], much attention has been attracted by quasicrystals, a unique type of structure, which lacks the translational symmetry but possesses certain orientational order. As the quasicrystal lattice structure in low dimension can be viewed as a projected pattern of the periodic lattice structure in higher dimension, a point-like Bragg diffraction arises as a natural result of such projection theory. The structural ordering of quasicrystals lies at the boundary between the translationally invariant crystals and random glassy materials. Much research work has been carried out in the past twenty years, among them the one dimensional model systems described by the Fibonacci sequences have received the most attention [2–5] since they contain the basic ingredients of quasicrystals and are relatively easy to deal with. Fibonacci system is famous for its Cantor-set spectrum (self-similarity) and critical eigenstates. One type of deterministically disordered system, Thue-Morse sequence, which is neither periodic, random nor quasiperiodic, is notable for its extended states (lattice-like field distributions) [6,7]. Another type of deterministically disordered system, period-doubling sequence, sharing common characteristics with both Fibonacci sequence (the spectra are Cantor-sets) and Thue-Morse sequence (their Fourier spectra are singular continuous), is also of great interest for its features [8] from theoretical point of view. Up to now, much work has been devoted to the electronic [9–11], vibrational [12,13], photonic [14–17], plasmon- polaritonic [18] properties in period-doubling systems, and all the above systems except the last concern only one degree of freedom. Little work has been done for phonon-polaritonic properties in piezoelectric period-doubling superlattices, which is to be studied in this paper and involves the coupling between photon and phonon.

In a periodic system, the spectrum is absolutely continuous and all the states are extended. The point of view that the spectrum of a disordered system has point singularities and all the states should be localized was prevailing. But as we nowadays know, correlated disorder can produce extended electronic states in one dimensional disordered system due to the existence of certain type of short range clustering effect among the atoms [19,20]. Such kind of dimer effect is also responsible for the extended electronic states in quasiperiodic copper-mean chain [21,22] and period-doubling lattice [11]. Although there are no dimers obviously in Thue-Morse sequence, extended electronic states also appear in this system, which was confirmed numerically by Ryu et al. [6] and understood by

[a] e-mail: zhenxingliu@hotmail.com

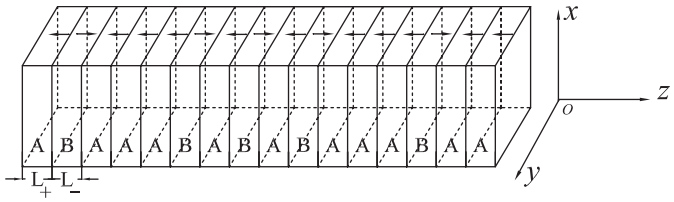

Fig. 1. The schematic diagram of a period-doubling piezoelectric superlattice. Domains' polarizations are along $\pm z$-axis, the electric field and vibrational displacement are taken as x-axis.

another kind of correlated disorder (clustering effect) [7]. In piezoelectric period-doubling superlattices to be discussed in this paper, extended phonon-polaritonic states also show up but can not be explained by the previous dimer effect because the extended states are actually lattice-like, nevertheless they can be explained with the similar mechanism taking place in Thue-Morse sequences. Our numerical as well as analytic calculations show that the lattice-like field distributions are a common feature of any sequence made of piezoelectric material and they result from the intrinsic properties of the corresponding transfer matrices for the particularly chosen frequencies.

In this paper, we consider the propagation of the electromagnetic wave through the piezoelectric superlattices with period-doubling sequences, the 4th-order period-doubling superlattice is illustrated in Figure 1, and the samples can be prepared with electric-field poling method [23]. The positively and negatively polarized domains with thickness $L_\pm$ are the two building blocks A and B, these building blocks are then arranged according to the period-doubling sequence. One simplest way to generate a period-doubling sequence is to follow the successive substitution $A \to AB$, $B \to AA$. Repeated substitution gives the following sequence: $A \to AB \to ABAA \to ABAAABAB \to ABAAABABABAAABAA \to \ldots$ The lth-order period-doubling sequence contains $N = 2^l$ blocks and the general recursive relations for the lth order are: $S_l = S_{l-1}S_{l-2}S_{l-2}$. In the piezoelectric period-doubling superlattices, we shall address the following two physical issues: (1) the branching rules of band-gap structure, which are not explored in previously studied period-doubling systems [9–18]; (2) the coexistence of lattice-like extended polaritonic states and critical states. Although periodic extended states are found in the period-doubling chain of the on-site model, nonperiodic (not lattice-like) extended states are found in the mixed model of the electronic systems studied previously [11] and in dielectric systems lattice-like extended states only appear at completely transparent frequencies, the lattice-like polaritonic extended states at frequencies corresponding to the pass-band for every order and critical states at all the low band-gap edges still have their special features in the piezoelectric period-doubling superlattice studied in this paper.

To maximize the coupling between photons and phonons in piezoelectric superlattices, one needs to have a setting which corresponds to the largest component of piezoelectric tensor. Figure 1 is such a setting for $LiNbO_3$, both electric field $E_x(z,t)$ and lattice displacement $u_x(z,t)$ are in x-axis, the full dynamics of the system is described by the following coupled equation set [24]

$$\left(\frac{\omega L}{2\pi c_s}\right)^2 \bar{E}_x(\bar{z},\omega) = -\alpha\frac{\partial^2}{\partial\bar{z}^2}\bar{E}_x(\bar{z},\omega) - \beta\theta(\bar{z})\frac{\partial^2}{\partial\bar{z}^2}\left[\theta(\bar{z})\bar{E}_x(\bar{z},\omega)\right] + \beta\theta(\bar{z})\frac{\partial^3}{\partial\bar{z}^3}\bar{u}_x(\bar{z},\omega), \quad (1a)$$

$$\left(\frac{\omega L}{2\pi c_s}\right)^2 \bar{u}_x(\bar{z},\omega) = -\frac{\partial^2}{\partial\bar{z}^2}\bar{u}_x(\bar{z},\omega) + \frac{\partial}{\partial\bar{z}}\left[\theta(\bar{z})\bar{E}_x(\bar{z},\omega)\right]. \quad (1b)$$

The above equation set is written in a dimensionless form, the scaled variables and functions are defined as $\bar{z} = 2\pi z/L$, $\bar{u}_x(\bar{z},\omega) = 2\pi u_x(z,\omega)/L$, and $\bar{E}_x(\bar{z},\omega) = |d'_{15}(z)|E_x(z,\omega)$. $L = L_+ + L_-$ and $\theta(\bar{z}) = \pm 1$ identifies the left and right polarized domains. $c_s = 1/\sqrt{\rho s'_{55}}$ is transverse sound velocity of ferroelectric media. The two dimensionless material parameters are $\alpha = c^2/\bar{\epsilon}c_s^2$, $\beta = d'^2_{15}/\epsilon_0\bar{\epsilon}s'_{55}$. β is the electromechanical coefficient which describes the coupling strength between photons and phonons. $\bar{\epsilon}$ is the effective dielectric constant and the reduced piezoelectric component is given by $d'_{15}(z) = d_{15}(z) + d_{16}(z)s'_{55}/s'_{65}$. The reduced elastic moduli are given by $1/s'_{55} = s_{66}/(s_{55}s_{66} - s_{56}s_{65})$ and $1/s'_{65} = -s_{56}/(s_{55}s_{66} - s_{56}s_{65})$. For $LiNbO_3$ [25], $\alpha = 1.6 \times 10^8$, $\beta = 0.5923$. Note that the photon velocity is higher than the sound velocity by four orders of magnitude and their wavelengths set two different characteristic length scales in this system.

The above equations can be solved for homogeneous ferroelectric media. The general solution for each domain can be expanded within the corresponding four eigensolutions. Under the proper boundary conditions at domain interfaces, the electric field $\bar{E}_x$, vibrational displacement $\bar{u}_x$, as well as their derivatives $\bar{E}'_x$ and $\bar{u}'_x$ at interfaces can be expressed in terms of transfer matrices for the left and right polarized domains [24]

$$\begin{pmatrix} \bar{E}_x(\bar{L}_\pm,\bar{\omega}) \\ \bar{u}_x(\bar{L}_\pm,\bar{\omega}) \\ \bar{E}'_x(\bar{L}_\pm,\bar{\omega}) \\ \bar{u}'_x(\bar{L}_\pm,\bar{\omega}) \mp \bar{E}_x(\bar{L}_\pm,\bar{\omega}) \end{pmatrix} = M(\bar{L}_\pm,\bar{\omega}) \begin{pmatrix} \bar{E}_x(\bar{0},\bar{\omega}) \\ \bar{u}_x(\bar{0},\bar{\omega}) \\ \bar{E}'_x(\bar{0},\bar{\omega}) \\ \bar{u}'_x(\bar{0},\bar{\omega}) \mp \bar{E}_x(\bar{0},\bar{\omega}) \end{pmatrix}. \quad (2)$$

$\bar{\omega} = \omega L/2\pi c_s$ and the detailed expressions of transfer matrices are listed in Appendix A of reference [24], the transfer matrix of a given superlattice can be obtained by successive multiplications of $M(\bar{L}_\pm,\bar{\omega})$ with the prescribed sequence. Equation (2) forms the basis to study band-gap structure and field distributions of this system.

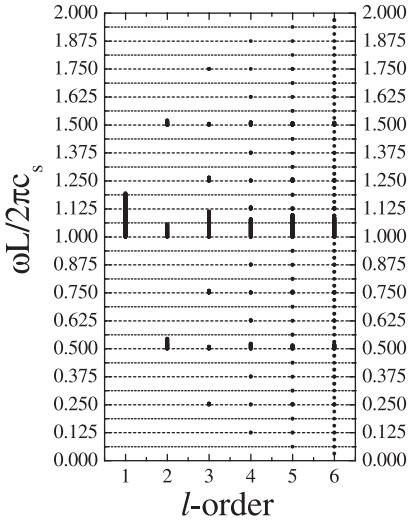

Fig. 2. Polaritonic band-gaps as a function of the order l of period-doubling superlattices. The reduced domain sizes are $\bar{L}_+ = \bar{L}_- = \pi$.

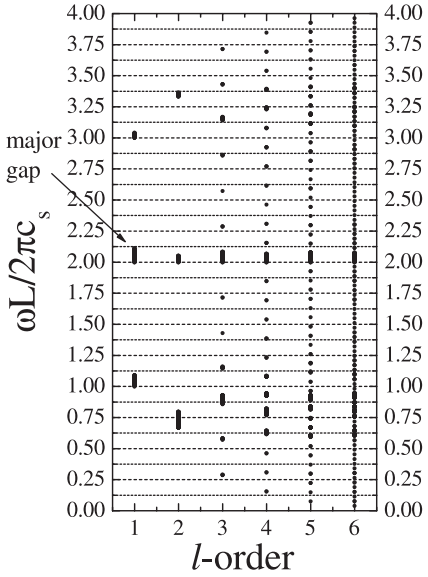

Fig. 3. Polaritonic band-gaps as a function of the order l of period-doubling superlattices. The reduced domain sizes are $\bar{L}_+ = 0.5\pi$, $\bar{L}_- = 1.5\pi$. One major gap is indicated.

The band-gap structure for a given period-doubling superlattice is calculated, as customarily done, under the periodic boundary condition. The typical band-gap structure for symmetrical setting ($\bar{L}_+ = \bar{L}_- = \pi$) is shown in Figure 2 where horizontal axis denotes the order l while vertical axis denotes the forbidden gap resulting from the superlattice structure. The band-gaps instead of pass-bands are plotted because they have potential application in photonic devices. It should be mentioned that the band-gap only acts on the coupled polaritons while uncoupled acoustic modes remain propagation-like. Actually there are many big clusters in the band-gap structure (the corresponding reason will be given below). To have a better view of spectral pattern, only the first big cluster in the range $\bar{\omega} = 0{-}2$ is shown. Figure 2 shows that the gap starts from around $\bar{\omega} = 1$ for the 1st order and is splitted into three subgaps, the middle gap persists for every order and the upper and lower ones are then further subdivided into three subgaps, and this process continues further on. In other words, the spectrum shows trifurcation and self-similarity. The number of subgaps included in the first big cluster of the lth-order symmetrical period-doubling piezoelectric sequence is $N_l = 2^l - 1$. The big clusters are separated by $\bar{\omega} = 2\times$integer and modes at $\bar{\omega} = 2\times$integer are all propagating-like for every order.

Above trifurcation pattern in the band-gap structure can be easily understood within the framework of plane wave expansion method. In the first-order approximation, the band-gap is opened in the neighborhood of reduced frequency $\bar{\omega} = |K_{m_l}|$ and the band-gap size approximately equals $(1/2)\beta|\theta(m_l)|^2|K_{m_l}|$, where $\theta(m_l)$ is the Fourier component of piezoelectric modulation $\theta(\bar{z})$ in the supercell and K_{m_l} is the reciprocal lattice vector. Thus, the nonvanishing Fourier components $\theta(m_l)$ yield directly the band-gap position. For a supercell composed of the lth-order symmetrical period-doubling sequence, the lattice constant is $a_l = 2^{l-1}2\pi$, the corresponding reciprocal lattice vector is given by $K_{m_l} = m_l/2^{l-1}$ and $m_l = -\infty \ldots + \infty$. The existence of polaritonic band-gap at $\bar{\omega} = |m_l/2^{l-1}|$ is simply determined by $\theta(m_l)$. Under periodic boundary condition, for every order of period-doubling sequence, a primary cell can be chosen to have even parity and $\theta(\bar{z})$ can be expanded into cosine series. The Fourier coefficients for the symmetrical period-doubling sequences can be calculated analytically and they are listed in Appendix A. Every Fourier coefficient includes a factor $\sin\frac{m_l\pi}{2^l}$ and vanishes at $m_l = 0, 2^l, 2\times 2^l, 3\times 2^l, \ldots$, the band-gap disappears at $\bar{\omega} = (0, 2, 4, 6, \ldots)$ accordingly. This is the reason why the spectrum trifurcates and forms clusters which are separated by even integer frequencies $\bar{\omega} = 0, 2, 4, \ldots$

However, such trifurcation scheme of the spectrum pattern happens only in the symmetrical setting. In the asymmetrical case ($\bar{L}_+ \neq \bar{L}_-$), the sample length of the $(l{+}1)$th order does not simply double that of the lth order and the reciprocal lattice vector needs not to be half of the previous order. Thus, the cluster pattern is somewhat different, but locations and sizes of the gaps still comply with the Fourier coefficients qualitatively. As an example, the band-gap structure for the asymmetrical case $\bar{L}_+ = 0.5\pi$ and $\bar{L}_- = 1.5\pi$ is illustrated in Figure 3. By comparing with the symmetrical case shown in Figure 2, one observes that the band-gap structure still forms big clusters, but now big clusters are separated by frequencies $\bar{\omega} = 0, 4, 8, \ldots$ instead of $\bar{\omega} = 0, 2, 4, \ldots$ because the gaps for every order disappear at $\bar{\omega} = 4, 8, 12, 16, \ldots$ And only the indicated major gap persists for every order unlike in the symmetrical case the middle subgaps persist for every order.

It is of interest to focus on those even integer frequencies $\bar{\omega} = 2, 4, 6, \ldots$ where band-gaps disappear for every order and to take a close look at the field distributions at these frequencies. The field distributions of electric field and vibrational displacement are plotted in Figure 4

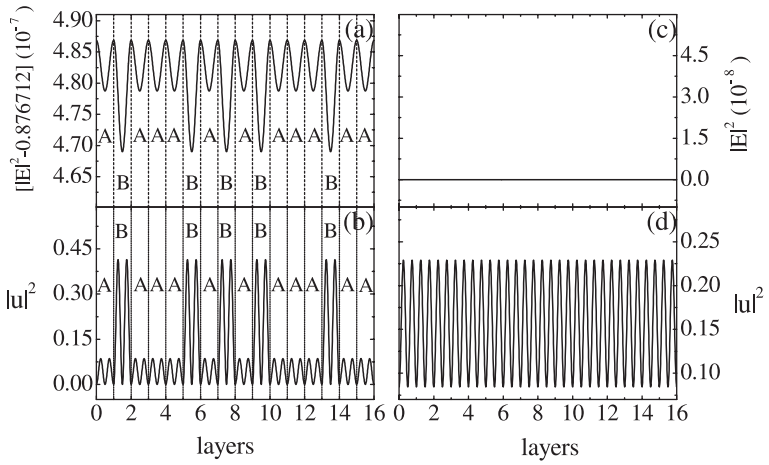

Fig. 4. Field distributions of the 4th-order period-doubling superlattice at $\bar{\omega} = 2$. The reduced domain sizes are $\bar{L}_+ = \bar{L}_- = \pi$. Left panel is for coupled polaritonic branch and right panel is for uncoupled acoustic branch. (a) and (c) Electric field; (b) and (d) Lattice displacement.

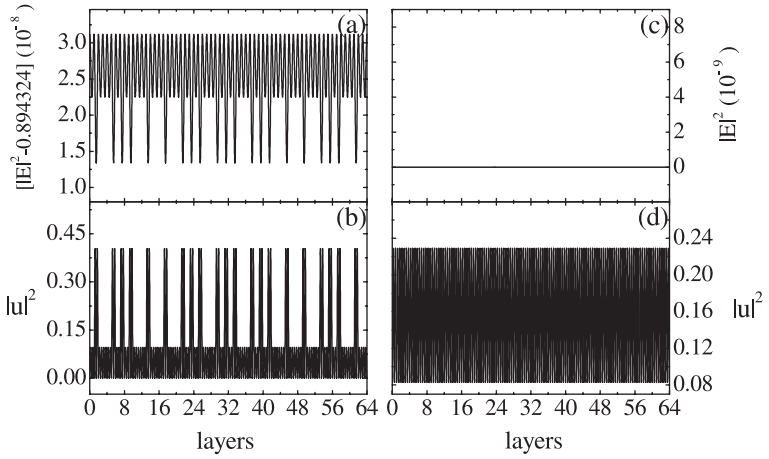

Fig. 5. Field distributions of the 6th-order period-doubling superlattice at $\bar{\omega} = 2$. The other parameters and notations are the same as in Figure 4.

for the symmetrical 4th-order period-doubling sequence of piezoelectric superlattice ($\bar{L}_+ = \bar{L}_- = \pi$) at $\bar{\omega} = 2$. Due to the photon and phonon degrees of freedom, two branches of field distribution exist: the left column is for the polaritonic branch and the right column is for the decoupled phononic branch. The upper panel is for electric field distribution and the lower panel is for vibrational displacement distribution. It is apparent that the phononic branch is Bloch-wave-like while the polaritonic branch of field distribution evidently resembles the 4th-order period-doubling sequence *ABAAABABABAAABAA*. This suggests that the polaritonic branch has the lattice-like field distribution and is characterized as extended. To check whether the conclusion is universal for every order of sequence, the field distribution for the symmetrical 6th-order sequence at $\bar{\omega} = 2$ is drawn in Figure 5. The polaritonic branch of field distribution still resembles the corresponding sequence of the 6th order. It is well-known that lattice-like field distribution is an icon feature of Thue-Morse sequence and correlated disorder (clustering effect) is responsible for its occurrence. The physical reason underlying such lattice-like field distribution is embedded in the dynamical matrices of the building blocks M_A and M_B. By calculating the commutator (M_A and M_B) as a function of frequency, we find that the commutator does vanish just around $\bar{\omega} = 2$. To be exact, the M_A and M_B commute with each other at $\bar{\omega} = 2.000000002548$ and the frequency deviates from $\bar{\omega} = 2$ obtained in zeroth order of dynamical matrices by β/α. At this specified frequency, M_A and M_B can have a pair of common eigenvectors. One of the eigenvectors corresponds to the pure phononic branch and thus uncoupled vibrational displacement distribution is Bloch-wave-like. The other eigenvector belongs to the coupled polaritonic branch, multiplying the matrices M_A and M_B on the coupled eigenvector yields the same magnitudes of electric field and vibration displacement, the stress component and the phase of electric field are somewhat different and lattice-like field distribution results from such matrix properties. We calculate the lattice-like states of higher-order piezoelectric period-doubling sequence at this precise frequency and find that the magnitudes of the states remain constant.

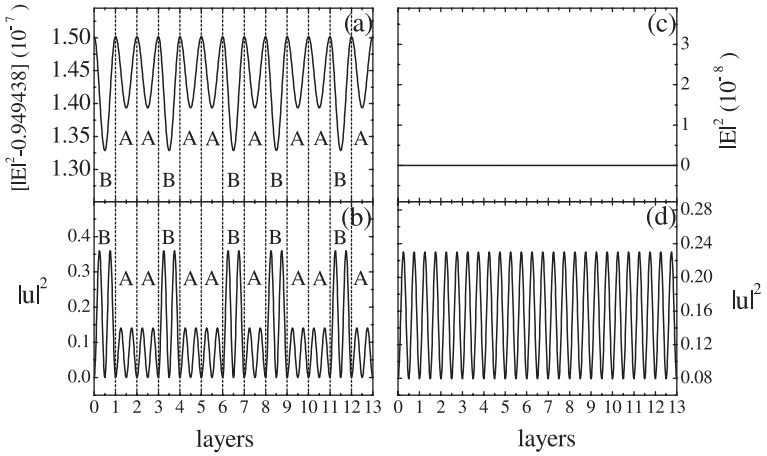

Fig. 6. Field distributions of the 6th-order Fibonacci superlattice at $\bar{\omega} = 2$. The other parameters and notations are the same as in Figure 4.

Since the matrix properties discussed above only depend on the reduced frequency and whether domain widths for the two polarized domains are equal, the lattice-like and Bloch-wave-like field distributions should be a universal feature and be irrespective of the lattice sequence type. To check this conclusion, field distribution of the 6th-order symmetrical Fibonacci piezoelectric sequence (13 domains) is given in Figure 6 for $\bar{\omega} = 2$. Field distribution of polaritonic branch in the left column does have the lattice-like field distribution pattern and resembles the sequence $BAABAABABAABA$ while that of purely phononic branch in the right column has the Bloch-wave-like behavior.

Another interesting feature worthy of investigation is the critical states at all the low band-gap edges $\bar{\omega} = |m_l/2^{l-1}|$ where strong coupling takes place between electromagnetic wave and acoustic wave. In the symmetrical period-doubling piezoelectric superlattice, the existence of the polaritonic band-gap around $\bar{\omega} = 1$ prohibits the propagation of coupled polaritonic branch, thus we focus on the propagative branch. In Figure 7, the field distribution of electric field of the propagative branch of the 5th–10th orders are shown and compared at the band-gap edge $\bar{\omega} = 1$. Evidently, the field distributions of all odd orders belong to one family and those of all even orders belong to another family, and each family forms a Cantor set. Members of one family are similar to each other, which becomes more apparent when the parts indicated by rectangles are enlarged. These states are characterized as critical. Note that the classification of field distributions into two different families are due to the different symmetries of period-doubling sequences in the families.

In conclusion, the propagation of electromagnetic wave in piezoelectric period-doubling superlattice is studied with generalized 4×4 transfer matrix method. For the symmetrical setting with equal domain thickness, the band-gap structure trifurcates under periodic boundary condition. At frequencies corresponding to the pass-band for every order, the phononic branch of field distribution is Bloch-wave-like and the polaritonic branch is lattice-like,

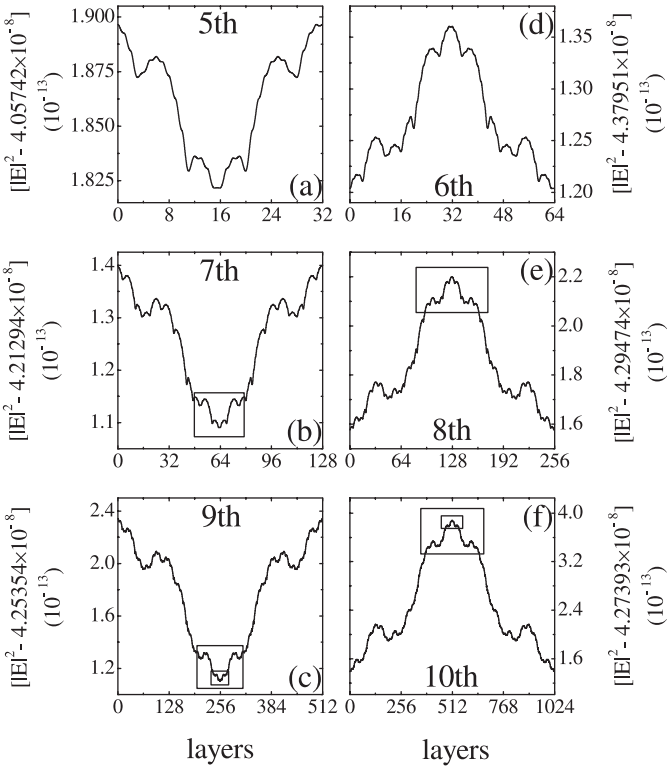

Fig. 7. Electric field of propagative branch of the 5th–10th-order period-doubling superlattices at $\bar{\omega} = 1$. The reduced domain sizes are $\bar{L}_+ = \bar{L}_- = \pi$. Left panel is for odd orders and right panel is for even orders.

which similar to those in the Thue-Morse sequence. Such lattice-like states can be characterized as extended if the superlattice size considered is large enough. Our study also suggests that the lattice-like field distributions are common phenomena in piezoelectric superlattices irrespective of lattice types and only depend on the frequency and domain widths. At all the low band-gap edges, the critical states appear in the propagative branch which form Cantor set separately for the even and odd-order families.

This work was supported in part by the State Key Program for Basic Research of China (Grant Nos. 2007CB925104, 2004CB619003). We wish to acknowledge the partial financial support from the NNSFC under Grant Nos. 10474040, 10334090, 10523001, and "Excellent Youth Foundation" [10025419].

Appendix A

Fourier coefficients $\theta(m_l)$ for the lth-order symmetrical period-doubling sequences:

$$\theta(m_1) = \frac{1}{2\pi}\int_0^{2\pi}\theta(\bar{z})\cos(m_1\bar{z})d\bar{z} = \frac{2}{m_1\pi}\cos m_1\pi \sin\frac{m_1\pi}{2}, \quad (A.1)$$

$$\theta(m_2) = \frac{1}{4\pi}\int_0^{4\pi}\theta(\bar{z})\cos\left(\frac{m_2}{2}\bar{z}\right)d\bar{z} = \frac{2}{m_2\pi}\cos m_2\pi \sin\frac{m_2\pi}{4}, \quad (A.2)$$

$$\theta(m_3) = \frac{2}{m_3\pi}\cos m_3\pi \sin\frac{m_3\pi}{8}\left[1+2\cos\frac{m_3\pi}{2}\right], \quad (A.3)$$

$$\theta(m_4) = \frac{2}{m_4\pi}\cos m_4\pi \sin\frac{m_4\pi}{16}\left[1+4\cos\frac{m_4\pi}{2}\cos\frac{m_4\pi}{4}\right], \quad (A.4)$$

$$\theta(m_5) = \frac{2}{m_5\pi}\cos m_5\pi \sin\frac{m_5\pi}{32} \times\left[1+2\cos\frac{m_5\pi}{2}\left(1+4\cos\frac{m_5\pi}{4}\cos\frac{m_5\pi}{8}\right)\right], \quad (A.5)$$

$$\theta(m_6) = \frac{2}{m_6\pi}\cos m_6\pi \sin\frac{m_6\pi}{64}\left[1+4\cos\frac{m_6\pi}{2}\cos\frac{m_6\pi}{4} \times\left(1+4\cos\frac{m_6\pi}{8}\cos\frac{m_6\pi}{16}\right)\right], \quad (A.6)$$

$$\theta(m_7) = \frac{2}{m_7\pi}\cos(m_7\pi)\sin\frac{m_7\pi}{128}\left\{1+2\cos\frac{m_7\pi}{2} \times\left[1+4\cos\frac{m_7\pi}{4}\cos\frac{m_7\pi}{8}\left(1+4\cos\frac{m_7\pi}{16}\cos\frac{m_7\pi}{32}\right)\right]\right\}, \quad (A.7)$$

$$\theta(m_8) = \frac{2}{m_8\pi}\cos m_8\pi \sin\frac{m_8\pi}{256}\left\{1+4\cos\frac{m_8\pi}{2}\cos\frac{m_8\pi}{4} \times\left[1+4\cos\frac{m_8\pi}{8}\cos\frac{m_8\pi}{16}\left(1+4\cos\frac{m_8\pi}{32}\cos\frac{m_8\pi}{64}\right)\right]\right\}. \quad (A.8)$$

By deduction, for odd order l:

$$\theta(m_l) = \frac{2}{m_l\pi}\cos m_l\pi \sin\frac{m_l\pi}{2^l} \times\left\{1+2\cos\frac{m_l\pi}{2}\left[1+4\cos\frac{m_l\pi}{4}\cos\frac{m_l\pi}{8} \times\ldots\left(1+4\cos\frac{m_l\pi}{2^{l-3}}\cos\frac{m_l\pi}{2^{l-2}}\right)\ldots\right]\right\}. \quad (A.9)$$

For even order l:

$$\theta(m_l) = \frac{2}{m_l\pi}\cos m_l\pi \sin\frac{m_l\pi}{2^l} \times\left\{1+4\cos\frac{m_l\pi}{2}\cos\frac{m_l\pi}{4}\left[1+4\cos\frac{m_l\pi}{8}\sin\frac{m_l\pi}{16} \times\ldots\left(1+4\cos\frac{m_l\pi}{2^{l-3}}\cos\frac{m_l\pi}{2^{l-2}}\right)\ldots\right]\right\}. \quad (A.10)$$

References

1. D. Shechtman, I. Blech, D. Gratias, J.W. Cahn, Phys. Rev. Lett. **53**, 1951 (1984)
2. M. Kohmoto, L.P. Kadanoff, C. Tang, Phys. Rev. Lett. **50**, 1870 (1983)
3. S. Ostlund, R. Pandit, D. Rand, H.J. Schellnhuber, E.D. Siggia, Phys. Rev. Lett. **50**, 1873 (1983)
4. R. Merlin, K. Bajema, R. Clarke, F.-Y. Juang, P.K. Bhattacharya, Phys. Rev. Lett. **55**, 1768 (1985)
5. G. Monsivais, J.A. Otero, H. Calás, Phys. Rev. B **71**, 064101 (2005)
6. C.S. Ryu, G.Y. Oh, M.H. Lee, Phys. Rev. B **46**, 5162 (1992)
7. A. Chakrabarti, S.N. Karmakar, R.K. Moitra, Phys. Rev. Lett. **74**, 1403 (1995)
8. E.L. Albuquerque, M.G. Cottam, Phys. Rep. **376**, 225 (2003)
9. J.M. Luck, Phys. Rev. B **39**, 5834 (1989)
10. J. Bellissard, A. Bovier, J.-M. Ghez, Commun. Math. Phys. **135**, 379 (1991)
11. A. Chakrabarti, S.N. Karmakar, R.K. Moitra, Phys. Rev. B **50**, 13276 (1994)
12. D.H.A.L. Anselmo, A.L. Dantas, S.K. Medeiros, E.L. Albuquerque, V.N. Freire, Physica A **349**, 259 (2005)
13. D.H.A.L. Anselmo, A.L. Dantas, E.L. Albuquerque, Physica A **362**, 289 (2006)
14. M.S. Vasconcelos, E.L. Albuquerque, Phys. Rev. B **59**, 11128 (1999)
15. Xiaoguang Wang, U. Grimm, M. Schreiber, Phys. Rev. B **62**, 14020 (2000)
16. M.E. Mora-Ramos, V. Agarwal, J.A. Soto Urueta, Microelectronics Journal **36**, 413 (2005)
17. H. Aynaou, E.H. El Boudouti, Y. El Hassouani, A. Akjouj, B. Djafari-Rouhani, J. Vasseur, A. Benomar, V.R. Velasco, Phys. Rev. E **72**, 56601 (2005)
18. M.S. Vasconcelos, E.L. Albuquerque, Phys. Rev. B **57**, 2826 (1998)
19. D.H. Dunlap, H.-L. Wu, P.W. Phillips, Phys. Rev. Lett. **65**, 88 (1990)
20. A. Sánchez, E. Maciá, F. Domínguez-Adame, Phys. Rev. B **49**, 147 (1994)
21. M. Severin, M. Dulea, R. Riklund, J. Phys.: Condens. Matter **1**, 8851 (1989)
22. S. Sil, S.N. Karmakar, R.K. Moitra, A. Chakrabarti, Phys. Rev. B **48**, 4192 (1993)
23. M. Yamada, N. Nada, M. Saitoh, K. Watanabe, Appl. Phys. Lett. **62**, 435 (1993)
24. Weiyi Zhang, Zhenxing Liu, Zhenlin Wang, Phys. Rev. B **71**, 195114 (2005)
25. Y. Nakagawa, K. Yamanouchi, K. Shibayama, J. Appl. Phys. **44**, 3969 (1973)